Direct Observation of Complete Fermi Surface, Imperfect Nesting, and Gap Anisotropy in the High-Temperature Incommensurate Charge-Density-Wave Compound $SmTe_3$

G.-H. Gweon,[1] J. D. Denlinger,[1] J. A. Clack,[1] J. W. Allen,[1] C. G. Olson,[2] E. DiMasi,[1,*] M. C. Aronson,[1] B. Foran,[3,†] and S. Lee[3,‡]

[1]*Randall Laboratory of Physics, University of Michigan, Ann Arbor, Michigan 48109-1120*
[2]*Ames Laboratory, Iowa State University, Ames, Iowa 50011*
[3]*Dow Laboratory of Chemistry, University of Michigan, Ann Arbor, Michigan 48109-1055*

(Received 10 March 1998)

We have carried out angle resolved photoemission spectroscopy of $SmTe_3$, a quasi-two-dimensional material with an incommensurate high-temperature charge density wave (CDW). This is the first direct experimental view of the full detail of an imperfectly nested Fermi surface, and the momentum space gap anisotropy, for an incommensurate CDW. [S0031-9007(98)06715-5]

PACS numbers: 71.45.Lr, 71.18.+y, 79.60.–i

Fermi surface (FS) energy gap formation is a fundamental quantum phenomenon in solids because thereby the system of interacting electrons can stabilize a broken symmetry ground state. Two important examples of such ground states are the superconducting state and the charge density wave (CDW) [1,2] state. In the superconducting state, the gap opens up due to formation of Cooper pairs. In the CDW state, the gap opens up due to formation of electron-hole pairs with wave vector $\vec{q}_{\mathrm{CDW}}$. The wave vector connects ("nests") one large portion of FS with another and dictates a new periodicity in the CDW state. In both cases, the gap momentum dependence is of central theoretical importance.

Angle resolved photoemission spectroscopy (ARPES) is a beautifully direct method to measure the momentum dependence of the gap if the gap is large enough to be energy resolved and if the material surface is stable for a long enough time to make the measurement. For a very few of the high-temperature superconducting cuprates it has been possible to measure [3] the gap momentum anisotropy so well as to permit meaningful comparison to microscopic theories. However, in spite of continuing efforts in various materials [4], comparably detailed ARPES studies of CDW gaps have not yet been made successfully. This is largely due to the lack of a material with both a big enough gap and a sufficiently stable surface.

This paper reports a detailed ARPES study of the CDW gap in $SmTe_3$, a novel incommensurate CDW material with a large anisotropic gap and very stable surface. We show below that the observed gap size implies a mean field transition temperature $\approx$1300 K, even larger than the melting temperature 1096 K [5], making $SmTe_3$ truly a "high-temperature CDW material." This is the first time that the nesting condition and the momentum dependence of a CDW gap have been tracked over the entire FS.

$SmTe_3$ is a layered material with conductivity anisotropy as big as 5000 [6]. The crystal structure as probed by x-ray diffraction [6] belongs to the orthorhombic group *Cmcm*, and consists of alternating SmTe and double Te layers, as shown in Fig. 1(a). It is known [6] that metallic electrical conduction occurs in the double Te layer. Remarkably, transmission electron microscope (TEM) diffraction patterns show, even at room temperature, satellites which are interpreted as due to incommensurate

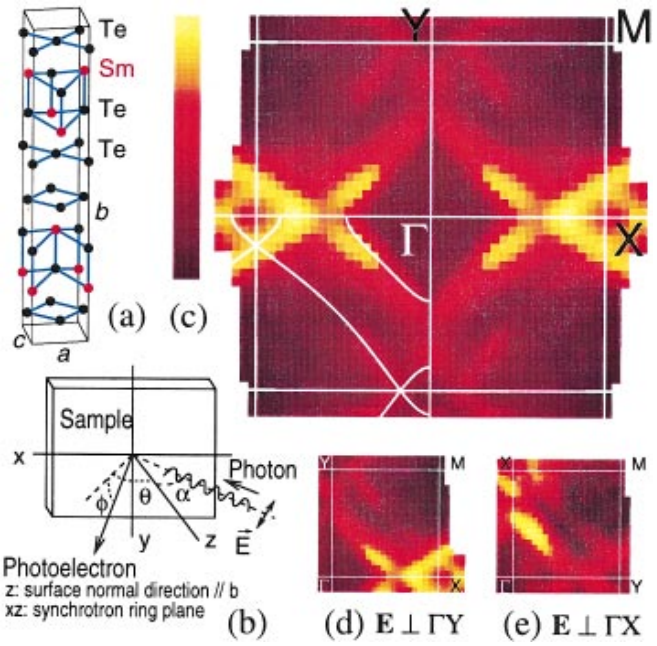

FIG. 1(color). (a) Schematic diagram for the one-face centered orthorhombic unit cell of $SmTe_3$ [6]. The dimensions are $a = 4.3326$ Å, $b = 25.6970$ Å, and $c = 4.3363$ Å. (b) Schematic geometry of the photoemission experiment. Photons with polarization $\vec{E}$ in the x-z plane propagate at fixed angle $\alpha \approx 45°$, relative to the sample surface normal z. (c) Fermi energy intensity map. $\Gamma X \parallel x$ in (b). The lengths of ΓX and ΓY could be either π/a and π/c or π/c and π/a. A theoretical FS is shown in the third quadrant. (d) Raw data for the map of (c), which is obtained by xy reflections of this map. (e) Map taken after the sample was rotated by 90° in the xy plane and then recleaved. The maps of (d) and (e) consist of 725 and 723 data points, respectively.

 0031-9007/98/81(4)/886(4)$15.00

CDW formation in the Te layers [7,8], with $\vec{q}_{\mathrm{CDW}} \approx \frac{2}{7} a^*$ or $\frac{2}{7} c^*$. The temperature dependencies of the magnetic susceptibility and the electrical resistivity show no anomalies from room temperature down to 1.2 K.

The single crystal samples were grown in RbCl-LiCl flux as described in Ref. [6]. The ARPES was performed at the Ames/Montana beam line of the Synchrotron Radiation Center (SRC) at the University of Wisconsin. Our sample orientation by Laue diffraction did not distinguish the very slight orthorhombicity [Fig. 1(a) caption]. The sample was cleaved *in situ* just before the measurement, which was done at room temperature and at pressure $\approx 4 \times 10^{-11}$ Torr. Monochromatized photons of energy 21.2 eV were used for all measurements reported here with one exception (see Fig. 2). The Fermi energy (E_{F}) and instrumental energy resolution were calibrated with a reference spectrum taken on a freshly sputtered Pt foil. The instrumental energy resolution ΔE was 140 meV FWHM for measurement of Fermi energy intensity maps and 50 meV FWHM for energy distribution curves (EDC's). The angular resolution for the spectrometer was $\pm 1°$, which amounts to $\pm 5\%$ of the distance from Γ to X in the Brillouin zone.

The FS geometry has been studied by making a momentum space E_{F} intensity map, a method introduced for the high-temperature cuprate superconductors [9]. In our experimental geometry, shown in Fig. 1(b), the map is obtained by sweeping angles ϕ (angle between the photoelectron momentum and its projection p_{xz} in the xz plane) and θ (angle between the z axis and p_{xz}). Because of translational invariance parallel to the surface, the photohole momentum parallel to the surface $\vec{k}_{\parallel}$ is the same as $\vec{k}_{\parallel}$ of the photoelectron, and so is determined unambiguously by these angles and the kinetic energy of the photoelectron. The FS pattern is generated because the intensity at E_{F} reaches a local maximum when a dispersing peak passes through the FS. However, a real ARPES experiment is characterized by a window with momentum and energy widths Δk and ΔE, set by instrumental angle and energy resolution, respectively. A dispersing peak contributes to a local maximum in the intensity map to the extent that the peak occupies the window, considering also the peak's intrinsic energy broadening and the relevant Fermi function. Depending on the specific details, a peak dispersing near to, but not crossing, E_{F} could contribute to the map, by either more or less than a peak actually crossing E_{F}. For the data presented below, gapped states near E_{F} do contribute to the intensity map, but less than the ungapped states.

Figures 1(c)–1(e) show E_{F} intensity maps. The logarithm of the intensity was used to enhance the weaker part of the image. The data are overplotted with the two-dimensional (2D) Brillouin zone of the crystal, labeled with notation for a 2D rectangular lattice. The full map 1(c) was generated by xy reflections of the raw data of map 1(d). The reflection symmetries, which are observed to hold in the raw data of 1(d), are valid symmetry operations for the orthorhombic crystal shown in 1(a).

In Fig. 1(c), we include in the lower left quadrant the theoretical FS obtained from extended Hückel tight binding bands calculated with the EHMACC program [10]. As in Ref. [7] the bands are for a single Te layer in $SmTe_3$ with 6.5 electrons per Te. In principle, each band is split by coupling to the other Te layer, but the data show only one evidence of such a splitting, pointed out further below. The slight difference in the a and c lattice parameters [Fig. 1(a) caption] is included in the calculation but is not visible in the results, which appear as perfectly fourfold symmetric. A detailed comparison of the theory and the experiment will be made below. For now, we simply note that there is a good general correspondence between all theoretical and experimental features, even though fourfold symmetry was not assumed in generating the experimental map. But, as we remarked above, one should not unconditionally interpret the pattern as showing the actual FS and it is noteworthy that in spite of its fourfold *shape*, the *intensity* variation is strongly twofold symmetric.

One could conjecture that the twofold symmetry involves the photoemission process in some way, e.g., selection rules involving the electron collection direction relative to the photon polarization. To test this possibility, maps 1(d) and 1(e) were taken for two sample orientations differing by 90°, by remounting and recleaving the same crystal. In both cases, the pattern is bright near the ΓX line and dim near the ΓY line. This shows unambiguously that the twofold symmetry is an intrinsic property of the crystal, not an extrinsic effect due to the photoemission process. We now show valence band EDC's which show *why* this twofold symmetry occurs.

Figure 2 shows ARPES spectra taken immediately after making the map of Fig. 1(c). Consistent results were obtained from a smaller set of EDC's taken after making the map of Fig. 1(e). The $\vec{k}$ values of the EDC's are shown as circles on the map. Along $X \rightarrow \Gamma$ in Fig. 2(a) three peaks (A, B, C) cross E_{F} at positions marked by the filled circles. We attribute the A-B splitting to the coupling between the Te layers. Along $Y \rightarrow \Gamma$, however, the three equivalent peaks (A', B', C') show gaps [11]. The size of the gap for electron removal is about 300 meV for A' and C'. The B' peak tends to merge with A' and we infer a similar gap size for both. Except for this gap vs crossing aspect, however, the same general behaviors obtain for all of the observed peaks in the EDC's for the two directions. A similar description holds along $X \rightarrow M$ and $Y \rightarrow M$ in Fig. 2(b), where the gap size is 300 meV for the peak A' and 260 meV for the peak B'. Other weakly dispersing peaks and shoulders at ~500 to 700 meV below E_{F} are plausibly ascribed to Te p states in the insulating SmTe layer.

The origin of the twofold symmetric intensity variation is now clear. For example, the large gaps along ΓY displace the dispersing peaks nearly out of the energy

window $\Delta E = 140$ meV so that the pattern is dim. Along ΓX with no gaps the pattern is bright. The fourfold symmetric shape of the map pattern is then interpreted as showing the "FS"—i.e., the FS that we would have obtained if there had been no gap—which we will give the precise shape of below. These findings connect naturally to a CDW picture, with the nesting wave vector as indicated in the map of Fig. 2(b). This wave vector is precisely the $\vec{q}_{\mathrm{CDW}}$ obtained from the TEM result [7], and gives the maximal nesting for our "FS." Figure 2(c) shows the gap anisotropy tracked over the two nested pieces of "FS." Along the outer "FS," $c \rightarrow e$, the emission intensity near d happens to be very weak at the photon energy used for the map and so these EDC's were taken instead at photon energy 17 eV, where the ARPES matrix element for the states is much larger. Note that the gap vanishes at d exactly where geometric nesting with the inner "FS" ceases. For the inner "FS," $a \rightarrow b$, the pattern becomes bright near b as the peak moves toward E_{F} into the energy window and the same would happen for the outer "FS" near b in a map taken at 17 eV. In short, our data show clearly the presence of the CDW state of $SmTe_3$. Further, the data imply a single $\vec{q}_{\mathrm{CDW}}$, at least over the ARPES sampling area ($\approx$0.1 mm^2) and depth ($\approx$15 Å). One can speculate that the crystal's slight orthorhombicity and the direction of $\vec{q}_{\mathrm{CDW}}$ are firmly linked, but large domains with $\vec{q}_{\mathrm{CDW}}$ along either ΓX or ΓY [7] are another possible scenario.

In the rest of this paper, we elaborate on details of imperfect nesting and gap formation of an incommensurate CDW as revealed by our data. Figure 3(a) shows FS crossings (circles) obtained from EDC's. Taking fourfold symmetry as approximately correct now, these crossings can be mapped to regions with gaps and used as anchor points to construct an experimental "FS" shown as white lines. For simplicity, the small A-B splittings have been ignored. This "FS" then determines the nesting wave vectors (arrows), $\vec{q}_{\mathrm{N}}$, which are *not* constant along the "FS." Figure 3(b) shows the electron removal gaps for the two paths a-b and c-d in Fig. 2(c) as a function of q_{N}. In general the two gaps are unequal.

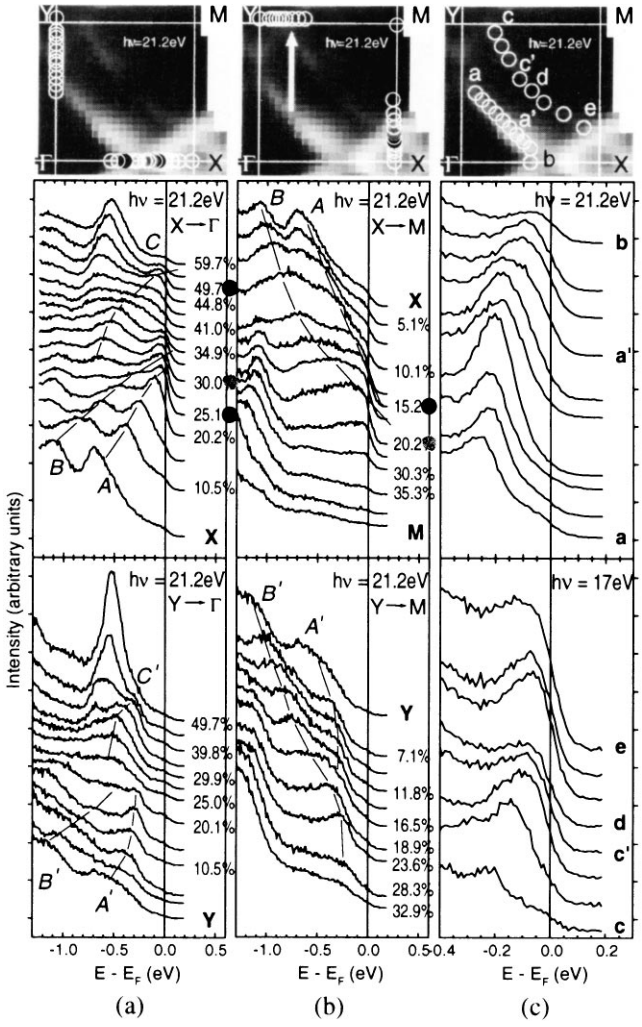

FIG. 2. Near E_{F} ARPES spectra for various cuts in momentum space. Each circle in the map corresponds to a spectrum in the plots below the map. The filled circles represent Fermi energy crossing points determined from dispersions. The size of the circles represents the size of the **k** resolution due to the finite angle resolution of the spectrometer. In (a) and (b), the **k** value for each spectrum is given in terms of the percentile distance along each symmetry line. In the map of (b), we show a nesting wave vector, consistent with our experiment and the TEM result [7]. (c) shows the gap anisotropy. The photon energy $h\nu = 21.2$ eV for all spectra, except the lower stack of (c), where $h\nu = 17$ eV to obtain adequate intensity near point d. All spectra are normalized to the photon flux, but each panel has a different overall scale.

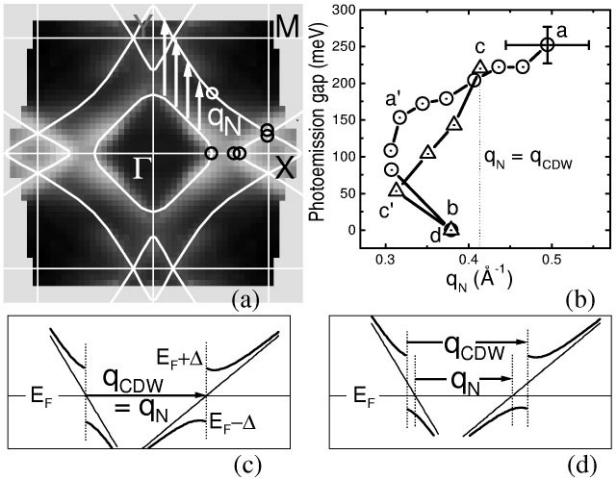

FIG. 3. (a) E_{F} crossing points (circles) from EDC's, experimental "FS" (white line), and nesting vectors (arrows), $\vec{q}_{\mathrm{N}}$, connecting "FS" pieces plotted over the E_{F} intensity map. (b) Electron removal gaps on the two "FS" pieces plotted as a function of q_{N}. The gap values are taken from the data of Fig. 2(c). Representative error bars are shown. (c),(d) Schematic diagrams showing two-band CDW mixing when $q_{\mathrm{N}} = q_{\mathrm{CDW}}$ and $q_{\mathrm{N}} < q_{\mathrm{CDW}}$. Δ mixes two states in the unperturbed bands (straight lines) connected by $\vec{q}_{\mathrm{CDW}}$, resulting in the gapped CDW bands shown as thick lines. The CDW bands are then folded back (not shown) according to the new periodicity.

Figure 3(c) illustrates the textbook scenario [2] of perfect nesting of two bands, shown with different E_F slopes as for $SmTe_3$. Because the inner FS band of Fig. 2(a) nests with an outer FS band that is the reflection, through the Y-M axis, of the one seen dispersing in Fig. 2(a), the two nesting bands have opposite slopes, as shown. For each pair of nested FS points $\vec{k}$ and $\vec{k} + \vec{q}_{CDW}$ one has a 2×2 degenerate matrix eigenvalue problem with off-diagonal matrix element Δ_k. The resulting E_F gap $2\Delta_k$ must be the same for both bands, as occurs for $SmTe_3$ *only* when $\vec{q}_{CDW} = \vec{q}_N$. Taking this electron removal gap of $\approx$200 meV to be Δ in the mean field relation $2\Delta = 3.52 k_B T_c$, one obtains $T_c \approx 1300$ K. Figure 3(d) shows the imperfect nesting situation where $q_N < q_{CDW}$. Because the unperturbed E_F slopes are unequal, the two bands now have unequal electron removal gaps, and one can show that the gaps have a linear dependence on $q_N(\vec{k}) - q_{CDW}$, as occurs from a to a' and from c to c' in Fig. 3(b). One also sees that previously unoccupied states are pulled below E_F. Similarly, for $q_N > q_{CDW}$, previously occupied states are forced above E_F. To maintain E_F in the gap and thereby achieve maximum CDW stability, electrons from the latter must exactly fill the former. One can show that the necessary condition on $\vec{q}_{CDW}$ is that

$$\sum_{q_N < q_{CDW}} [q_{CDW} - q_N(\vec{k})] = \sum_{q_N > q_{CDW}} [q_N(\vec{k}) - q_{CDW}].$$

Indeed, we find that this condition is satisfied to within 4% for our nesting "FS."

Thus this simple two-band model reproduces many of the experimental observations in Fig. 3(b). However, our preliminary analysis shows some quantitative disagreements, which calls for a multiband model including the double Te layer and the SmTe layer. Because of the approximate fourfold symmetry, a successful theory of the nested bands along ΓY should start with un-nested bands deduced from our EDC's along ΓX. A further challenge to a full theory is the apparent absence of any emission intensity from the "backfolded" bands in the gapped EDC's of Figs. 2(a) and 2(b). Such intensity was identified in recent ARPES studies of superconductor gap formation [12]. Lastly, a study of band symmetry properties as in Ref. [13] shows that near the point b the character of the inner FS band crosses over from p_x to p_y ($x \parallel \Gamma M$ and $y \parallel XY$), while near the point d the character of the outer FS band continues to be p_x. Because of this symmetry change, we expect that from a' to b and from c' to d, even though q_N becomes constant and then increases again, the gap will nonetheless continue to decrease before going to zero abruptly at b and d, as occurs in Fig. 3(b).

In conclusion, we have presented a detailed ARPES study on the FS shape and the anisotropic gap of $SmTe_3$, a high-temperature incommensurate CDW compound. The experimental "FS" shows an excellent agreement in shape with an extended Hückel tight binding band theory and shows a nesting property consistent with the TEM diffraction pattern [7]. The big gap size $\approx$200 meV implies a high transition temperature and enables a very detailed gap anisotropy study. The latter is discussed in terms of an imperfect nesting condition and the symmetry properties of the bands. Our results vividly illustrate how incommensurate CDW nesting occurs in a real quasi-2D material.

G.-H. G. is grateful to R. Claessen, W. P. Ellis, and F. Reinert for contributing to the early stages of this work. Work by G.-H. G., J. D. D., J. A. C., and J. W. A. at U-M was supported by the DOE under Contract No. DE-FG02-90ER45416 and by the NSF Grant No. DMR-94-23741. Work at the Ames lab was supported by the DOE under Contract No. W-7405-ENG-82. Work by E. D., M. C. A., B. F., and S. L. at U-M was supported by the NSF Grant No. DMR-9319196. The Synchrotron Radiation Center is supported by the NSF under Grant No. DMR-95-31009.

*Present address: Physics Dept., Brookhaven National Laboratory, Upton, NY 11973-5000.
†Present address: SEMATECH, 2706 Montopolis Dr., Austin, TX 78741-6499.
‡Present address: Baker Laboratory of Chemistry, Cornell University, Ithaca, NY 14853-1301.

[1] R. E. Peierls, *Quantum Theory of Solids* (Oxford University Press, New York, 1955).
[2] G. Grüner, *Density Waves in Solids* (Addison-Wesley, Reading, MA, 1994).
[3] Z.-X. Shen *et al.*, Phys. Rev. Lett. **70**, 1553 (1993); H. Ding *et al.*, Phys. Rev. B **54**, 9678 (1996).
[4] B. Dardel *et al.*, J. Phys. Condens. Matter **5**, 6111 (1993); A. Terrasi *et al.*, Z. Phys. B **100**, 493 (1996); R. Liu *et al.*, Phys. Rev. Lett. **80**, 5762 (1998).
[5] P. Villars and L. D. Calvert, *Pearson's Handbook of Crystallographic Data for Intermetallic Phases* (ASM International, Materials Park, OH, 1991), 2nd ed., Vol. 4.
[6] E. DiMasi *et al.*, Chem. Mater. **6**, 1867 (1994).
[7] E. DiMasi *et al.*, Phys. Rev. B **52**, 14 516 (1995).
[8] As often happens, the CDW satellites are too weak to be observed in x-ray diffraction, which lacks the sensitivity that multiple scattering imparts to electron diffraction.
[9] P. Aebi *et al.*, Phys. Rev. Lett. **72**, 2757 (1994).
[10] R. Hoffmann, J. Chem. Phys. **39**, 1397 (1963); M.-H. Whangbo *et al.*, Proc. R. Soc. London Ser. A **366**, 23 (1979); M.-H. Whangbo *et al.*, EHMACC program for extended Hückel molecular and crystal calculations.
[11] The gapped spectra in Fig. 2 display small but nonzero spectral weight near E_F due to the PES peak's linewidth tail (arising from thermal CDW fluctuations, from simple phonon broadening, or from the photoelectron lifetime), and possibly to some non-**k**-conserving scattering. We also calculate that when the gapped state above E_F is at its closest approach to E_F, as in the 20.1% spectrum of Fig. 2(a), the thermal occupation of its tail at 300 K can produce the weak but observable PES peak just at E_F.
[12] J. C. Campuzano *et al.*, Phys. Rev. B **53**, R14 737 (1996).
[13] B. Foran, Ph.D. thesis, University of Michigan, 1996.